TRANSPORT PROBLEMS 2022 Volume 17 Issue 1
PROBLEMY TRANSPORTU DOI: 10.20858/tp.2022.17.1.07

Keywords: aluminium alloys; non-alloy steel; laser welding, microstructure; structure

Karolina MISIURA[1], Jarosław KONIECZNY[2]*, Krzysztof LABISZ[3], Renata BORIS[4]

INVESTIGATIONS OF THE STRUCTURE AND HARDNESS OF DISSIMILAR STEEL-TO-ALUMINUM JOINTS MADE USING LASER WELDING TECHNOLOGY

Summary. Since welding technology is currently used to assemble the frame of driver's seats, it is important to develop laser welding technology for steel and aluminium. For this reason, the purpose of the present work was to examine the structure and selected properties of aluminium-steel joints using the example of an EN AW-6060 aluminium alloy and DC04 low-alloy steel welded in laser technology. Overlapping joints were made, weld type –following the hole laser welding method –laser beam (LB) using a high power disk laser (TRUMPF TruDisk3302), in which the active medium is a yttrium-aluminium crystal (YAG). Metallographic microstructure investigations were carried out using a light microscope from Carl Zeiss - Observer Z1m, and the weld microstructures were investigated using an SEM Supra 35 microscope, also from Carl Zeiss. The chemical composition analysis in micro-areas was carried out using an X-ray energy dispersion spectrometer from EDAX, which was a part of the SEM Supra 35. The hardness of the substrate material and the welded area was measured following the Vickers method using an FM-ARS 9000 micro hardness tester from Tokyo, Japan. It was found that there is a potential for commercial use of laser welding to make a low-carbon steel-aluminium alloy joint. During the formation of the weld in its microstructure, intermetallic compounds of the FexAly type were created, which significantly reduced the mechanical and plastic properties of the joint. The hardness of the weld created wasabout seven times higher than that of DC04 carbon steel. The choice of laser welding parameters (primarily, laser power and beam speed) significantly impacted the weld structure and properties.

1. INTRODUCTION

Car seats are one of the most important features determining comfort while driving. Maintaining a proper and comfortable driving position, which depends on the relative position of the steering wheel and seat, affects the safety of vehicle users. The standard car seat is made of tubes, metal mouldings, and sometimes light-alloy cast parts. All elements are connected to form the so-called armchair frame [1].

Currently, there is a tendency on the market to replace some structural parts of individual car elements with light materials. This is due to the desire to reduce the weight of the vehicle, which

[1]Silesian University of Technology; Konarskiego 18A, 44-100 Gliwice, Poland; email: karolina.karcz23@gmail.com; orcid.org/0000-0001-6246-2225
[2]Silesian University of Technology; Krasinskiego 8, 40-019 Katowice, Poland; email: Jaroslaw.Konieczny@polsl.pl; orcid.org/0000-0002-7318-5187
[3]Silesian University of Technology; Krasinskiego 8, 40-019 Katowice, Poland; email: Krzysztof.Labisz@polsl.pl; orcid.org/0000-0002-4613-830X
[4]Vilnius Gediminas Technical University; Linkmenų str. 28, Vilnius 08217, Lithuania; email: renata.boris@vgtu.lt; orcid.org/0000-0001-8819-955X
* Corresponding author. E-mail: jaroslaw.konieczny@polsl.pl

translates into reduced fuel consumption, thus reducing environmental pollution. In addition, reducing the weight of the car at the same engine power increases the maximum speed and improves driving dynamics [2, 3].

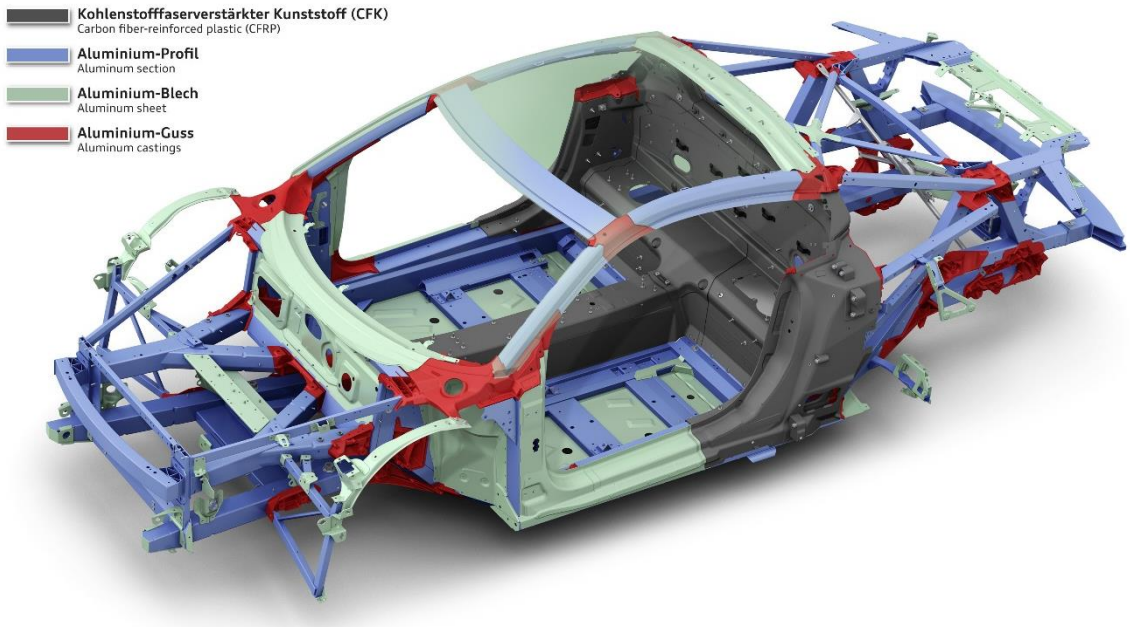

Fig. 1. An example of a hybrid car body in which steel elements are replaced with light materials such as aluminium alloys or carbon fibres [4]

The Audi A6 Coupé is a very good example of new construction solutions by which steel is replaced by materials of a lower density (and, thus, a lower weight), such as aluminium alloys and carbon fibres (Fig. 1). In the automotive industry, such replacements have been common for many years. Replacing all the steel parts with aluminium alloys in the body structure reduces the weight of a car by about 40%. This reduced weight increases the vehicle's manoeuvrability and driving comfort. In addition to aluminium alloy bodies, rims, heads and engine blocks, and suspension components are utilised in expensive cars.

Moreover, the use of materials such as low-carbon steel requires corrosion protection, while this is not the case for aluminium alloys, which are characterised by natural corrosion resistance. For these reasons, replacing some steel parts with aluminium in the driver's seat is a very good and perspective solution [5, 6].

Since welding technology is currently used to connect the metal elements of adriver's seat, it is important to develop laser welding technology for steel and aluminium. Therefore, the purpose of the current work was to examine the structure and selected properties of aluminium-steel welded laser technology joints on the example of EN AW-6060 alloys and DC04 steel.

2. MATERIALS AND METHODS

The weld was made during the laser welding of low-alloy, low-carbon steel for plastic working DC04 [7] and aluminium alloy for plastic working EN AW-6060 [8]. 1.2-mm-thick DC04 steel sheets and 2-mm-thick aluminium alloy sheets were welded. The chemical composition of steel is given in Tab. 1, and that of an aluminium alloy is given in Tab. 2.

The joint type was chosen following [9]. The joints were performed as the overlap joint type using bore laser welding technology- laser beam (LB).

Laser welded joints were made by putting the plates on a metal laser table, with an aluminium plate on the bottom and a steel plate on top of it. Both plates were pressed with a steel plate with a milled

elongated hole through which the laser beam fell directly on the DC04 low carbon steel plate. The laser head was tilted 3° to the axis (laser head-table) to prevent the laser beam from reflecting off the steel plate, which would have resulted in the beam returning to the laser head and damaging the lens. The joints were made using a high-power disk laser (TRUMPF TruDisk3302), in which the active medium is an yttrium-aluminium crystal (YAG) [10]. The parameters of laser welding are given in Tab. 3.

Table 1

Chemical composition of steel DC04 [7]

Concentration of the elements [%]			
C	Mn	P	S
Max 0.08	Max 0.40	Max 0.03	Max 0.03

Table 2

Chemical composition of the aluminium alloy EN AW-6060 [8]

Concentration of the elements [%]							
Si	Fe	Cu	Mn	Mg	Cr	Zn	Ti
0.30-0.6	0.10-0.30	0.10	0.10	0.35-0.6	0.05	0.15	0.10

Table 3

Laser welding parameters

Sample / Parameters	Weld speed(v)	Focus diameter (ϕ)	Laser power(P)	Focus length
Sample 1	0.5 m/min	200 μm	600 W	Focus of 3.2 mm over the surface of the steel plate.
Sample 2	0.5 m/min	200 μm	600 W	Focus lowering of 1 mm over the surface of the steel plate.
Sample 3	0.5 m/min	200 μm	1000 W	Without changes
Sample 4	0.5 m/min	200 μm	1000 W	Focus 1 mm higher over the surface of the steel plate.
Sample 5	0.5 m/min	200 μm	800 W	Without changes
Sample 6	0.4 m/min	200 μm	800 W	Without changes
Sample 7	0.3 m/min	200 μm	800 W	Without changes
Sample 8	0.5 m/min	200 μm	1200 W	Focus 1 mm higher over the surface of the steel plate

Metallographic microstructure investigations were carried out using a light microscope (Carl Zeiss Observer Z1m), and photos of the tested microstructure of welds were taken using a scanning electron microscope (SEM)(Carl Zeiss, Supra 35). The chemical composition of the micro-areas was analysed using an EDAX energy dispersion spectrometer.

The hardness of initial materials and welds was measured by applying the Vickers method using an FM-ARS 9000 micro hardness tester from Tokyo, Japan. Ten measures were taken for each hardness value.

3. RESULTS AND DISCUSSION

Because samples No. 1 and No. 2 were not permanently joined, no microstructure tests were performed. Based on the analysis of the laser welding parameters (Table 3), only increasing the power from 600 W to 1000 W ensured a durable joint of the tested materials. Preliminary results of testing sample No. 3 are presented in another work [11].

Fig. 2 shows the macrostructure of weld sample No. 4. The drop of the weld (Figs. 2a and 2b) and the high porosity of the weld (Fig. 2c) are clearly visible.

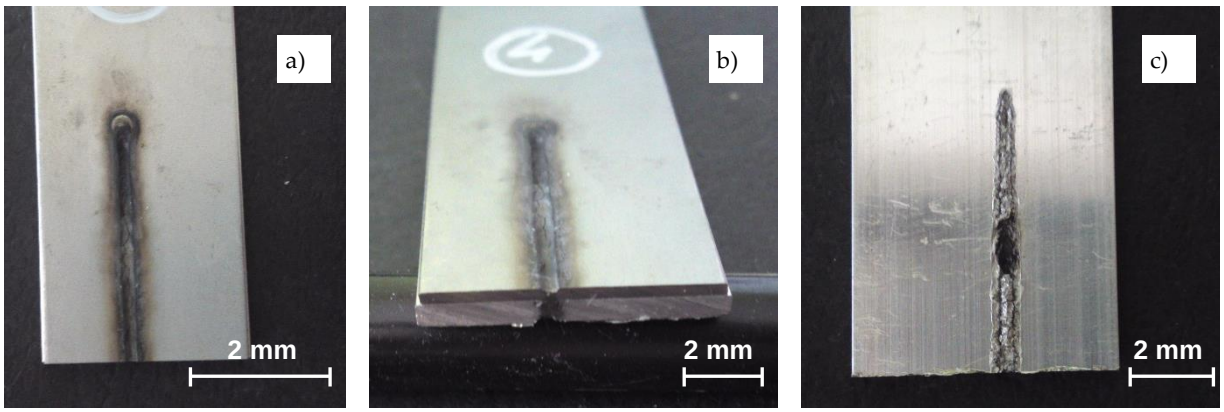

Fig. 2. Sunken weld face a) weld cross-section; b) weld ridge – high porosity visible; c) sample No. 4

The microstructure of sample joint No. 4 was analysed, and the results show the weld structure, DC04 steel plate, and EN AW-6060 aluminium alloy plate, as well as the transition zone. A crack running along the weld from the top to the bottom of the joint's cross-section, as well some shorter cracks inside the weld, are clearly visible. In addition, a clear boundary is visible between the weld and the steel plate. Meanwhile, the border between the weld and the material of the EN AW-6060 aluminium alloy plate is no longer clearly visible. From the analysis of the structure of the weld and changing its appearance from the top to the bottom of the cross-section, a change in its morphology is visible. This change suggests that its chemical and phase composition also change.

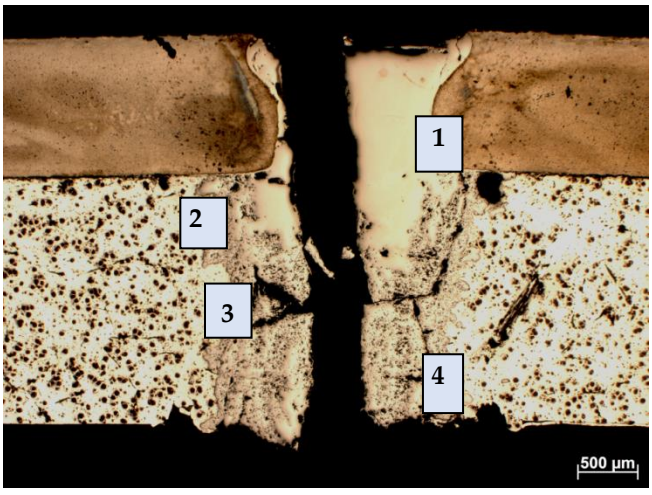

Fig. 3. Sample 4: Microstructure image of the weld join, light microscope image

Fig. 4 shows the enlarged areas 1-4 marked in Fig. 3. In area 1, the boundary between the DC04 steel material and the weld material is clearly visible. Dendrites are visible in the weld at the border. On the other hand, trans-crystalline inclusions and cracks are visible in the remaining areas. In addition, in areas 2-4, needles can be recognised in the form of needles characteristic of aluminium

alloy structures with the addition of silicon alloys. Silicon does not dissolve in aluminium alloys and creates pure needle-shaped silicon substances [12].

Fig. 5 presents a macro image of weld sample No. 6. The weld face is quite even (Fig. 5a), and only the weld ridge is characterised by high porosity (Fig. 5c).

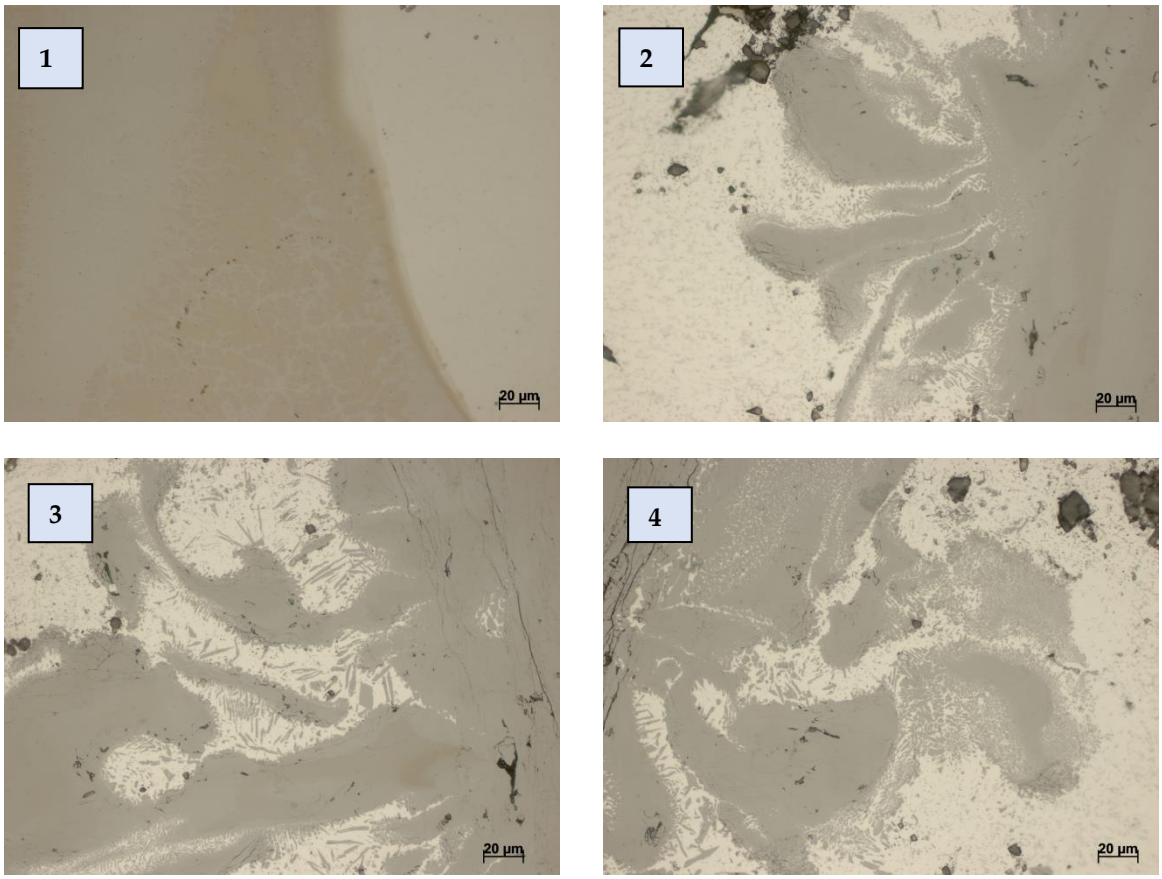

Fig. 4. Microstructures of the characteristic areas marked with numbers 1-4 in Fig. 3 from the edge of the weld, SEM

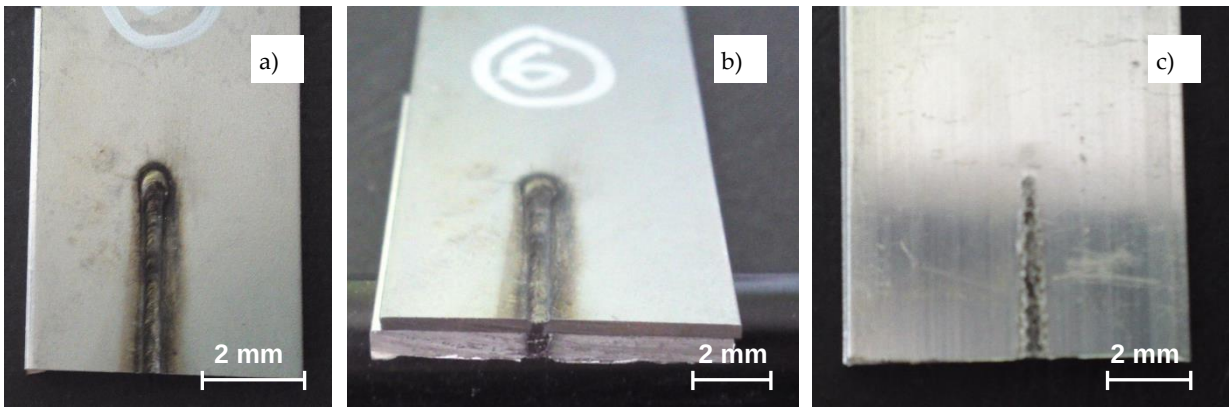

Fig. 5. Weld face a) weld cross-section; b) weld ridge – high porosity visible; c) sample No. 6

Fig. 6 shows the microstructure of the joint obtained after reducing the laser power from 1000 W to 800 W and reducing the welding speed by 0.1 m/min. Similar to sample No. 4, in this case, the boundary between the DC04 steel material and the weld material is clearly visible(see area 5 in

Fig. 7). Additionally, cracks in the weld material can be seen running along and across the boundary between the weld and the native material. Also, the dendrite precipitates in this sample are visible in the weld in area 5 (Fig. 7).

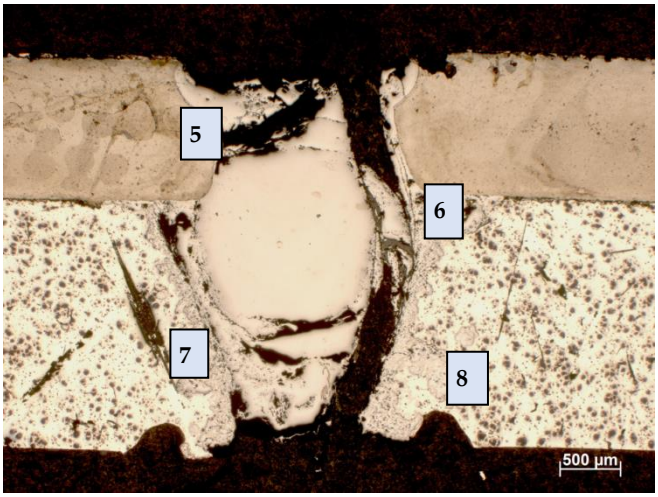

Fig. 6. Sample No. 6: Microstructure image of the joint LM

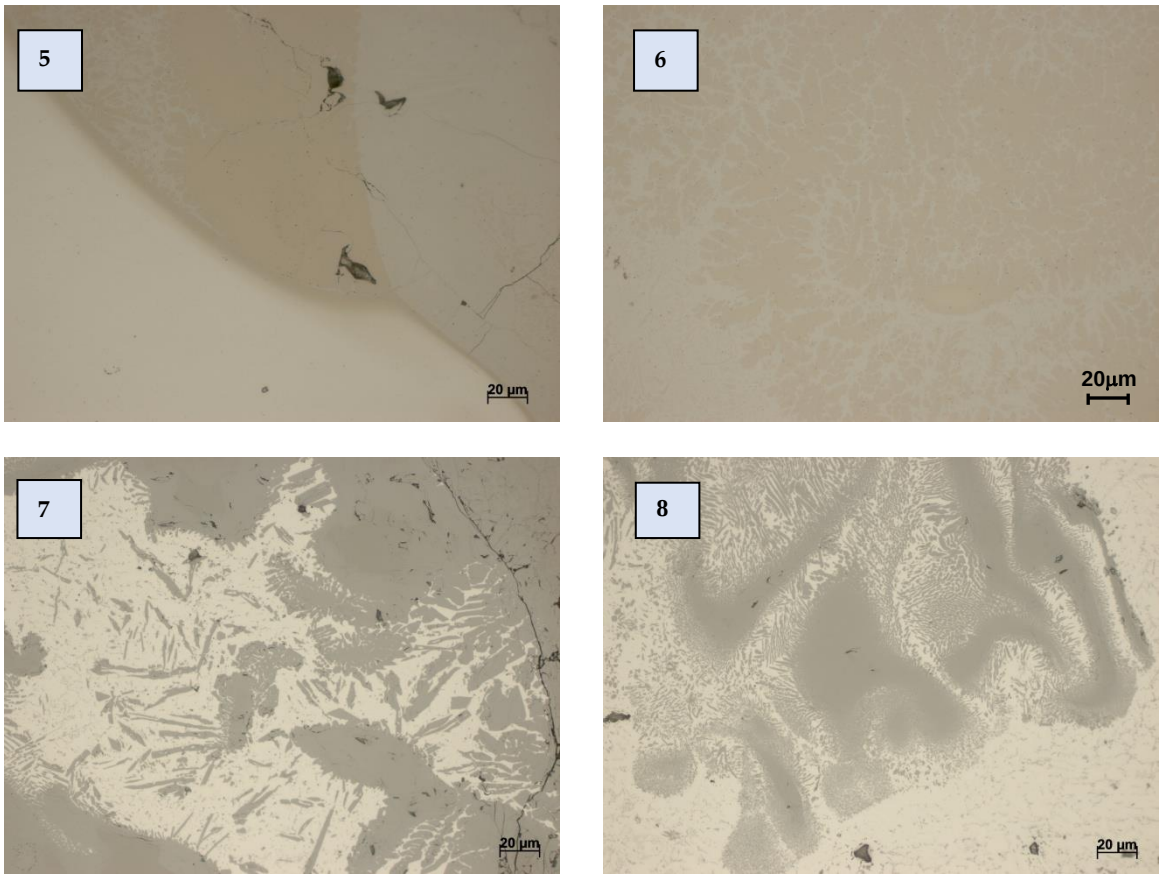

Fig. 7. Microstructures of the characteristic areas marked with numbers 5-8 in Fig. 6 from the edge of the weld, SEM

Meanwhile, a large trans-crystalline crack is visible on the right side of Fig. 7(area 7). In addition, in both areas, precipitations are visible in the form of needles as in Fig. 4. Also, in this case, these are most likely primary silicon precipitations characteristic of aluminium alloys with the addition of Si.

Fig. 8 shows a macro image of weld sample No. 8. The weld face is fairly even (Fig. 8a).However, the weld ridge is characterised by very high porosity (Fig. 8c). Only preliminary tests on the light microscope were performed for this joint (Fig. 9), as the weld was completely destroyed during laser welding. In this case, no SEM, chemical composition analysis, EDS, or micro hardness measurements were performed.

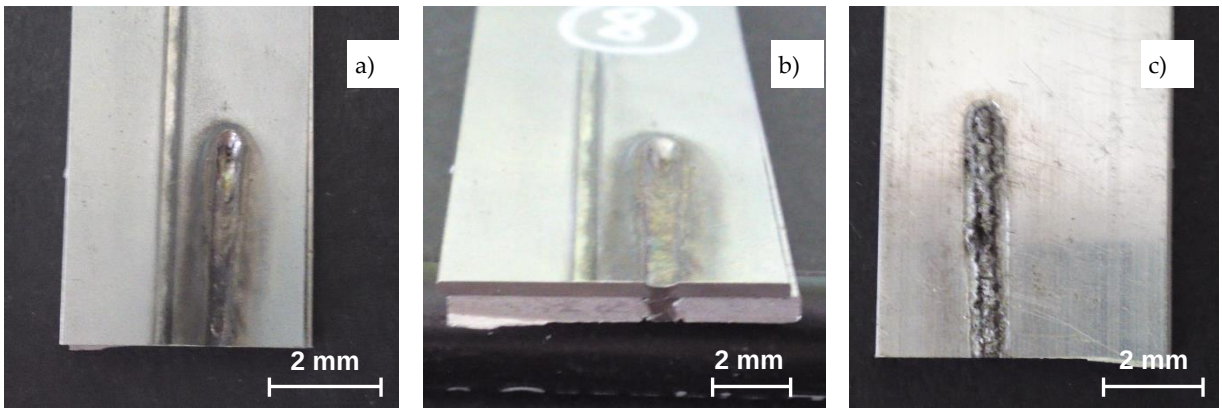

Fig. 8. Weld face a) weld cross-section; b) weld ridge – high porosity visible; c) sample No. 8

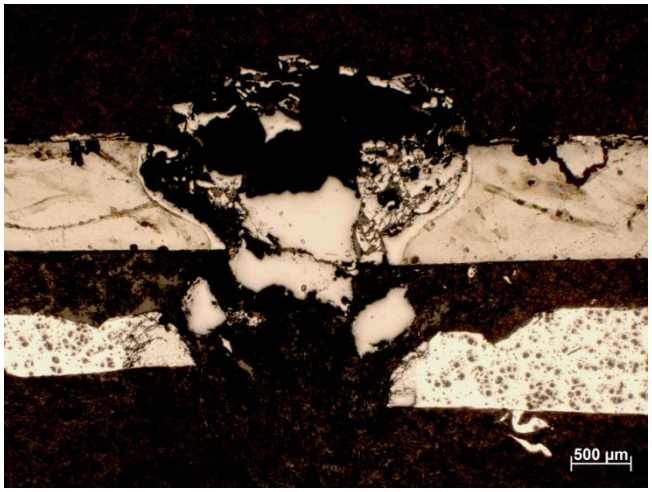

Fig. 9. Sample No. 8: Microstructure image of the join LM

In the next stage, tests were carried out using SEM, including microstructure observations and tests of chemical composition in EDS micro-areas. Also, measurements were taken of the hardness of DC04 steel joints and an EN AW-6060 aluminium alloy made using a high-power TRUMPF TruDisk3302 disk laser.

Fig. 10 shows the microstructure image of sample No. 4 obtained using an SEM. In area A (Fig. 11 a), the boundary between the DC04 steel substrate and the weld material is visible. Between these areas, a transition strip with a width of about 10 is visible. To the right of the border is the joint material; the nature and shape of this material's partitions are characteristic of aluminium alloys. Meanwhile, Fig. 11 a shows the area of substrate materials of DC04 steel and EN-AW-6060 aluminium alloy, as well as the weld area. Most of the precipitation and inclusions are characteristic of the aluminium alloy, less is characteristic of the weld, and the steel has practically no inclusions.

Fig. 12 presents the results of the chemical composition investigations of micro-areas. Iron (55.7 wt%) and aluminium (44 wt%), as well as a small amount of silicon (0.26 wt%), were found in the weld (Fig. 12c). Silicon oxide precipitations were also observed in the weld (Fig. 12d). Oxygen, silicon, and a small amount of aluminium were found in the native material of the aluminium alloy (Fig. 12b).

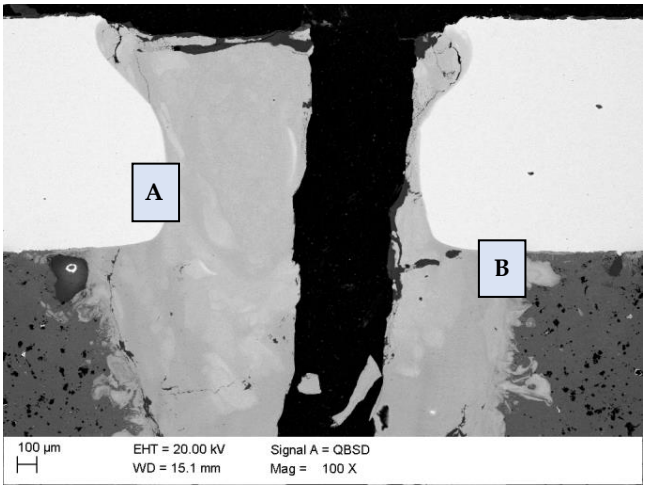

Fig. 10. Image of the top area of the weld, sample No. 4, SEM

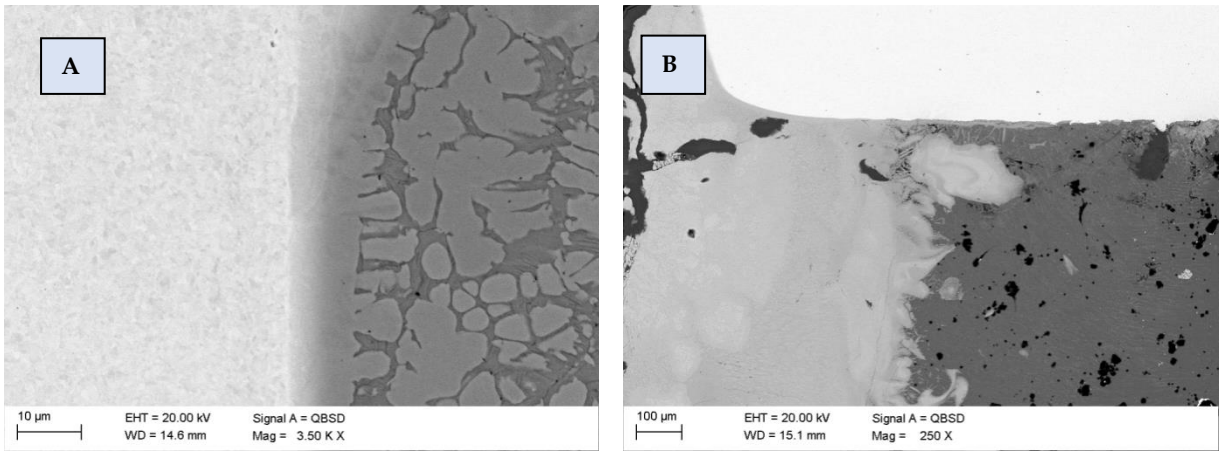

Fig. 11. Microstructure of the characteristic areas in Fig. 5: a) joining area of the DC04 steel with the EN AW-6060 aluminium alloy showing the phases of diverse materials; b) characteristic silicon precipitation in the bottom part of the weld

Next, the change in chemical composition along the steel-HAZ-weld (Heat Affected Zone) line was examined (Fig. 13). The iron concentration in the HAZ belt rapidly decreased between the DC04 material and the weld. However, at the same time, the concentration of aluminium increased rapidly. Furthermore, the weld material maintained a low, even iron content while the aluminium content changed. Similar results were obtained in previous works [13, 14].

The results of the weld structure observation of sample No. 6 and its central area are shown in Figs. 14a and b. A very large, destructive fracture of the weld on the left is visible, as are trans-crystalline cracks in its upper part of Fig. 14a. In contrast, the central weld area contains no cracks. Its structure shows dendritic separations, which are characteristic of both iron alloys and aluminium casting alloys (Fig. 14b).

The chemical composition analysis in the micro-areas revealed that only iron and aluminium were present in the weld near the HAZ (Figs. 15a and c). At the same time, it was found that the HAZ between the weld material and aluminium was not liquid; also, numerous precipitates were formed due to remelting (Fig. 15a). A HAZ analysis in the area of contact of steel, aluminium, and weld revealed the presence of aluminium, iron, and zinc (Fig. 15b). The presence of zinc can be explained by its participation in the chemical composition of the aluminium alloy EN AW-6060 (Table 2). The presence of silicon oxide with the addition of aluminium was also observed in HAZ (Fig. 15d).

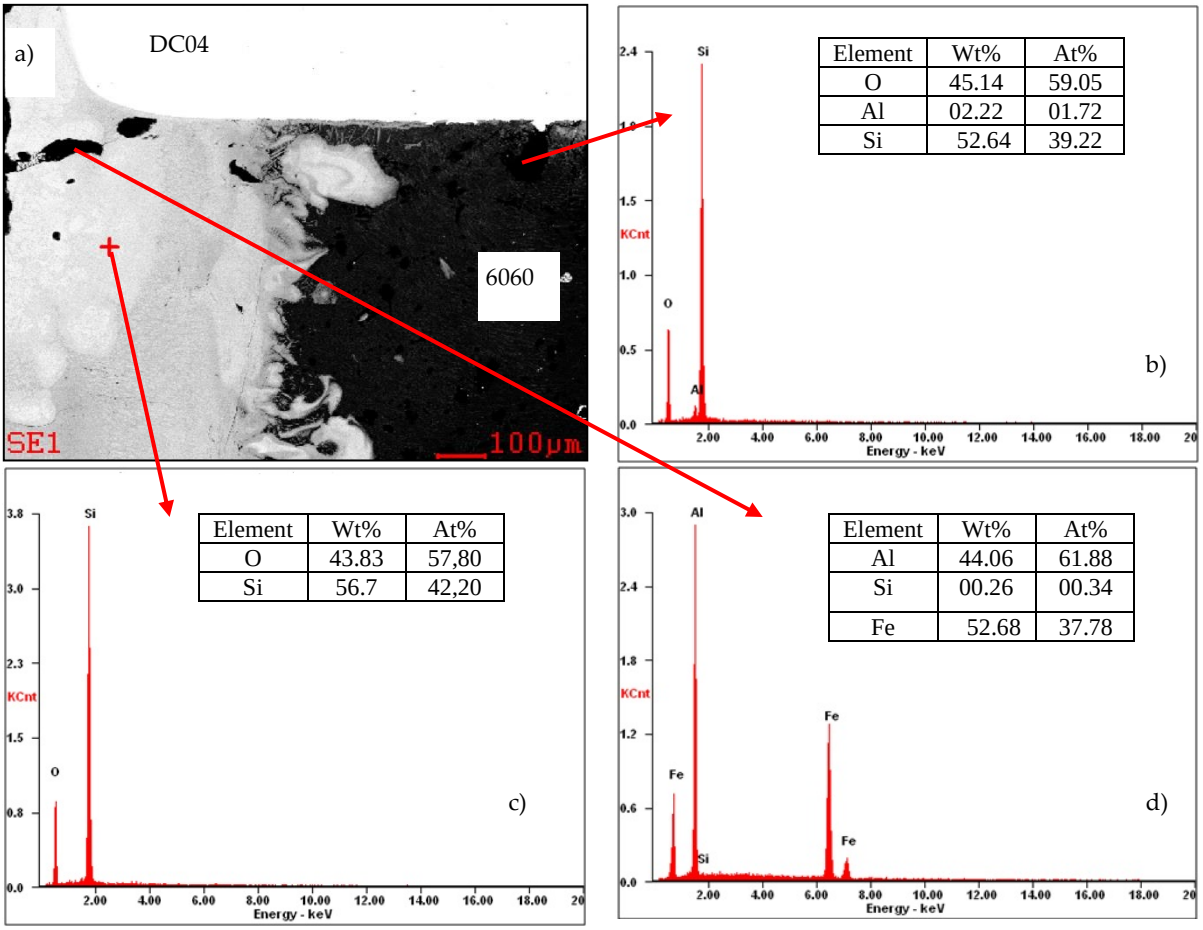

Fig. 12. a) SEM image of the joint weld structure between DC04 steel and an EN AW-6060 Al alloy and b-d) the EDS chemical composition analysis of the darker area, sample No. 3

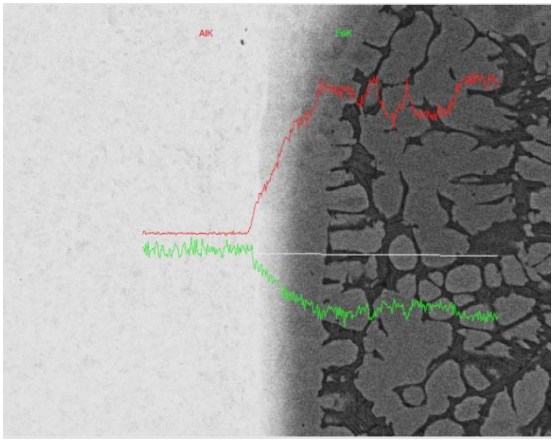

Fig. 13. EDS line analysis of the chemical composition, SEM, 20 kV, 2000x, sample No. 4

The EDS analysis for both samples showed the presence of silicon in HAZ. Oxygen was also present due to the high affinity of this element for both aluminium and silicon. Cracks running along the weld in the HAZ or in the weld itself are most likely the result of stress caused by the separation of intermetallic Fe_xAl_y phases, and small transcrystalline cracks are caused by the non-metallic inclusions that occurred on the edge of the weld.

In the next stage, the hardness of the matrix materials, HAZ, and weld were measured. Ten hardness measurements were recorded for each material, and the average value and standard deviation were calculated (Figs. 16, 17).

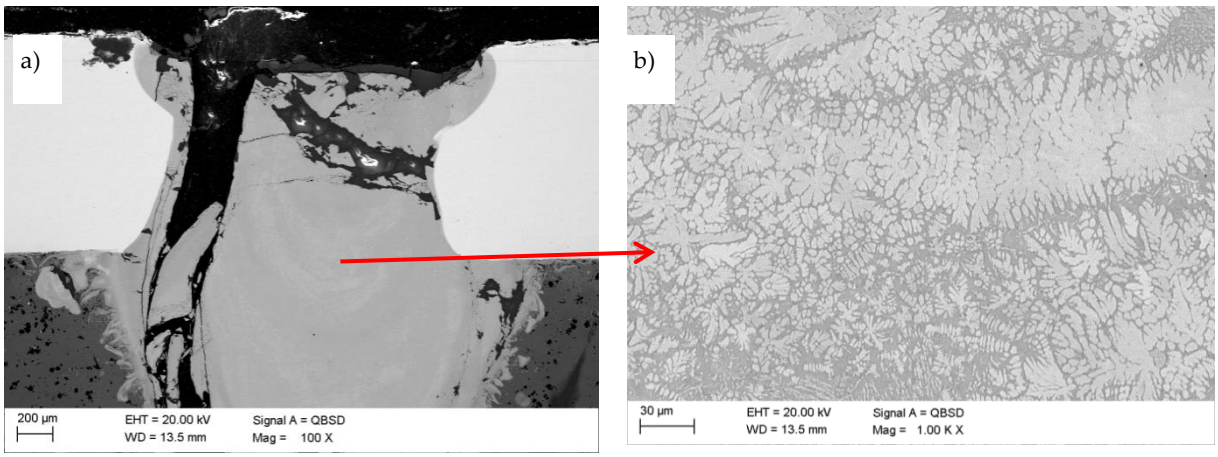

Fig. 14. The image of the upper area of the weld and a magnification of the area showing numerous cracks in the weld as well as silicon precipitations, sample No. 6, SEM

Based on the obtained results, the average hardness values of the EN AW-6060 alloy (up to 0.6571 GPa) and DC05 steel (1.03 GPa) were determined. Figs. 16a and b show the results of the measurements of the hardness of sample 4 and sample 6, respectively. In both cases, it can be seen that the hardness of the weld is about seven times higher than that of the native materials. This is most likely due to the formation of hard dendritic grains derived from FeAl intermetallic phases in the structure. A similar relationship was found in [13], where the hardness of the intermetallic layer was estimated at 9.8±0.9 GPa. The average hardness of the weld for sample No. 4 was 7.05 GPa; for sample 6, the average hardness was 7.25 GPa. This slight difference may be due to the use of various welding parameters, which caused structures to form with different chemical and phase compositions, as well as different volumes of FexAly intermetallic precipitates.

The combination of steel and aluminium by conventional welding methods is practically impossible, as the poor compatibility of these two materials generates many problems. When making this type of connection, the thermal expansion coefficient and melting point should be taken into account. During welding, the transition to liquid takes place during the formation of the weld. Then, at room temperature, the solubility of steel and aluminium is limited, which causes brittle FexAly intermetallic phases to form [14].

The results indicate that the brittle cracking of the welds generated was most likely caused by the brittle phases or intermetallic compounds that formed as a result of metallurgical reactions during the weld formation. The chemical composition investigations in micro-areas of samples No. 4 and No. 6 (Fig. 12 and Fig. 15) indicate that phases of the system Fe_xAl_y (Fe_3Al, FeAl, $FeAl_3$ or/and Fe_2Al_5) were created as a result of laser welding in the weld. Such phases adversely affect plastic properties and strength joints. The growth of the Fe_2Al_5 phase layer is controlled by a diffusion reaction and complies with the parabolic law, while the growth of the $FeAl_3$ layer is linear and controlled by an intermediate reaction [16].

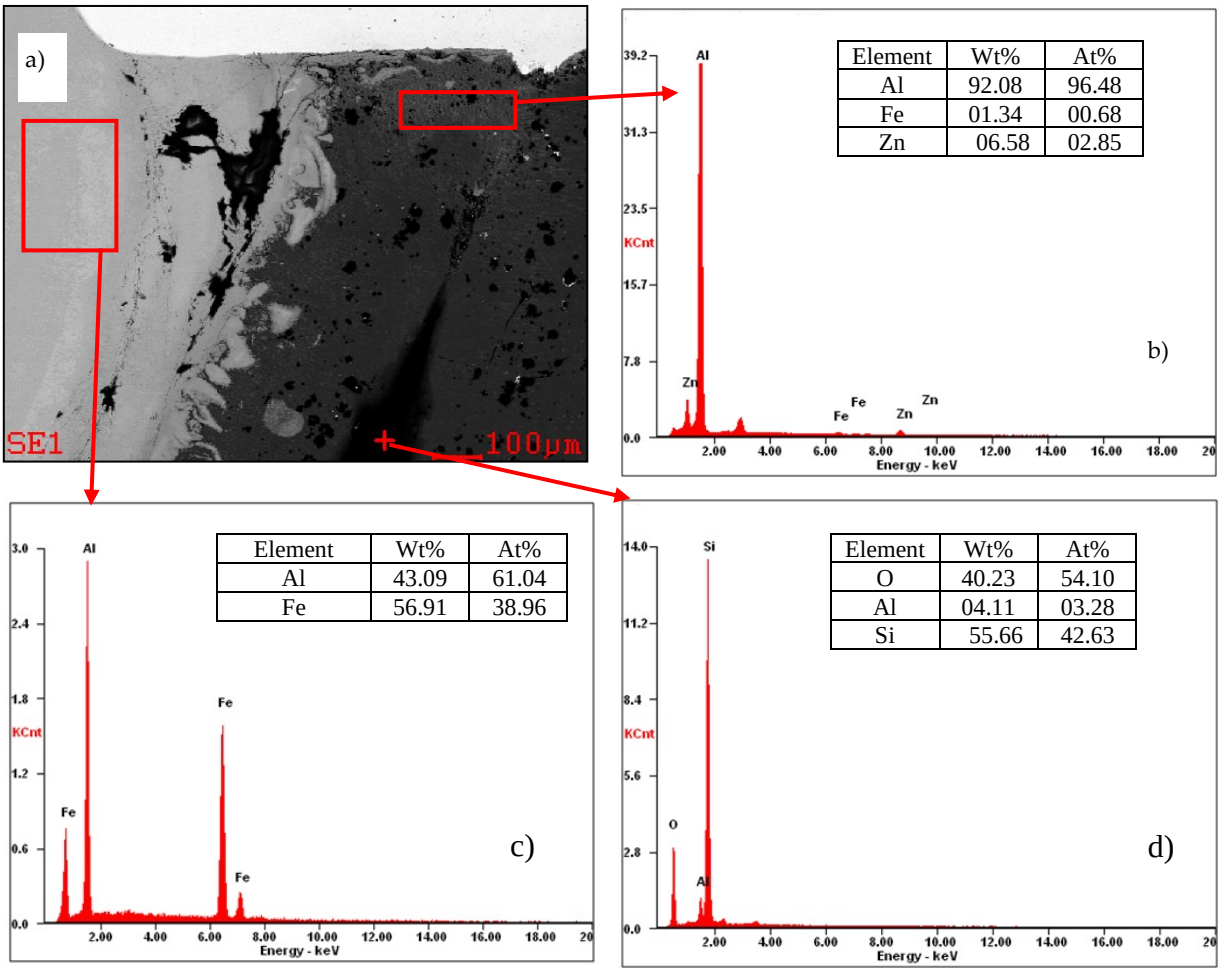

Fig. 15. Microstructure of the weld between DC04 steel and the EN AW-6060 aluminium alloy from the weld edge, as well as the EDS chemical composition microanalysis, sample No. 6, SEM

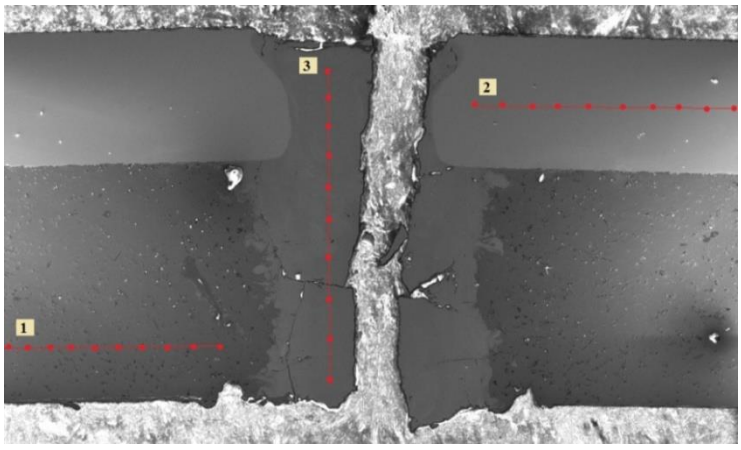

Fig. 16. Sample No. 4: Microhardness measurement diagram

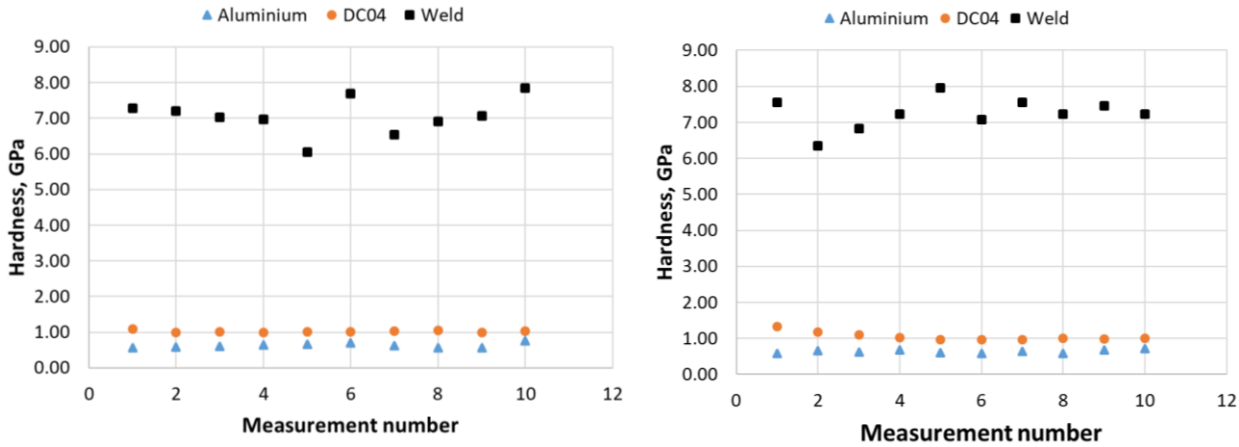

a) b)

Fig. 17. Hardness measurement results a) Sample No. 4; b) Sample No. 6

Due to the chemical composition of the EN AW-6060 alloy, silicon has a significant impact on the precipitation characteristics of the intermetallic phase. As the Si content in an aluminium bath increases, the Fe_2Al_5 and $FeAl_3$ phase growth rate decreases; meanwhile, the activation energy of Fe_2Al_5 decreases as the Si content in the bath increases [16].

The formation of a brittle intermetallic phase causes extensive cracks along the joint and depends on the heat supplied during welding [15]. Meanwhile, [17] observed that the precipitation of the $FeAl_3$ intermetallic phase on the aluminium side is needle-shaped, while the Fe_2Al_5 phase that occurs on the iron side takes the shape of tongues. Moreover, the precipitation of the intermetallic phase on the steel side is much thicker than that of $FeAl_3$ phases. An acceptable standard of intermetallic layer thickness in aluminium-steel joints is 10 μm.

Phases of this type are characterised by high hardness, which can reach values of up to 11.8 GPa, and low yield strength. This results in low mechanical properties of the formed joint. The thickness of this phase does not exceed 10 μm and is directly proportional to the amount of heat introduced – the more heat in the joint, the greater the area of the intermetallic phase. Therefore, when joining steel and aluminium, a tendency to continuously reduce the heat supplied in all possible methods was noted [15, 18]. According to [17, 19], the size of the intermetallic phase in the weld can be increased by increasing the laser power density.

The formation of the weld and the chemical and phase composition of the structure is the sole result of the diffusion process. In the first phase of the intermetallic phase, growth occurs on the aluminium side due to the diffusion of iron into aluminium. This process occurs only in the solid state of both metals (i.e. below the melting temperature of aluminium (T<660°C)). In contrast, embryo growth on the steel side takes place in the liquid phase of aluminium (T>660˚C). At this stage, significant nucleation of this phase is possible.

Significant amounts of iron diffused into the weld layer, which does not promote the formation of a correct joint, as it causes welding misalignments. The reason for the higher diffusion of metals from the DC04 sheet into the weld material is that diode laser welding is a high-energy method, meaning that high levels of energy are introduced into the joint.

As a result of welding, fine non-metallic inclusions appeared in the microstructure of the weld, which may be the site of crack initiation. However, microscopic observations indicate that, in most cases, crack initiation takes place in HAZ as in [14]. However, in the case of welded joints, the stress is usually concentrated in areas characterised by a lack of remelting, tearing at the edge of the weld face and partial melting. As a result of metallographic tests, partial remelting was noticed near the edge of the weld (Fig. 10 and Fig. 14).

Based on the shape of the weld face and ridge (Fig. 2 and Fig. 5), it can be concluded that the parameters of the obtained weld also depend on the location of the laser beam focus.

Due to the large electrochemical difference of 1.22 volts, different thermal and electrical conductivity, when welding steel and aluminium, numerous voids (cavities) and cracks formed in the weld [20].

Previously, [13] observed that, during the formation of the weld, when the reaction takes place in the liquid state (above the melting point of aluminium), the Fe-Al intermetallic phase first separates from the solidified Al as the primary phase. This is due to the solubility of Fe in aluminium, which is 2.5 ± 0.1 wt.% at 700°C [21], and the low energy of iron diffusion activation of 123.8 kJ/moll [22] in liquid Al.

As demonstrated in [23], the strength of steel-aluminium alloy welded joints increases as the width of the aluminium weld increases and decreases as the thickness of the intermetallic compounds layer decreases.

Previous researchers [19] have confirmed that when welding carbon steel and an aluminium alloy EN AW-6061, using Al5Si film as an interlayer reduces the formation of the IMC layer in the weld and reduces the size of the intermetallic phase precipitations to 2 μm. In addition, crack initiation and pore formation have been reduced.

4. CONCLUSIONS

As a result of the current investigation, the following results were found:

1. There is potential for the commercial use of laser welding to produce low carbon steel-aluminium alloy joints.
2. During the formation of the weld, intermetallic compounds of the Fe_xAl_y type are generated in its microstructure, which significantly reduces the mechanical and plastic properties of the joint.
3. The hardness of the created weld is about seven times higher than the basic material (carbon steel).
4. The choice of laser welding parameters (primarily laser power and beam speed) has a substantial impact on the structure and properties of the weld.
5. The requirement for a permanent connection is, besides the use of appropriate laser power (sample No. 1 and sample No. 2), also connected to the determination of the appropriate welding speed.

References

1. Kale, H.N. & Dhamejani, C.L. Design parameters of driver seat in an automobile. *International Journal of Research in Engineering and Technology.* 2015. Vol. 4(6). P. 448-452.
2. Steinwall, J. & Viippola, P. *Concept Development of a Lightweight Driver's Seat Structure & Adjustment System*. Department of Product and Production Development. Chalmers University of Technology. Gothenburg, Sweden. 2014.
3. Meszler, D. & German, J. & Mock, P. & Bandivadekar, A. Summary of mass reduction impacts on EU cost curves. *Working Paper* 2013-1. 2013. International Council on Clean Transportation (ICCT).
4. Audi MediaCenter. Leightweight Construction. Available at: https://www.audi-mediacenter.com/en/photos/album/leightweight-construction-240.
5. Kciuk, M. & Kurc, A. & Szewczenko, J. Structure and corrosion resistance of aluminium AlMg2.5; AlMg5Mn and AlZn5Mg1 alloys. *Journal of Achievements in Materials and Manufacturing Engineering.* 2010. Vol. 41(1-2). P. 74-81.
6. Labisz, K. & Konieczny, J. & Wierzbicki, Ł. & Ćwiek, J. & Butor, J. Influence of primary silicon precipitates on anodized aluminum alloys surface layer properties. *Transport Problems.* 2018. Vol. 13(2). P. 111-120.
7. PN-EN 10130:2009. *Cold-rolled flat products made of low-carbon steels for cold forming. Technical delivery conditions.*
8. PN-EN 573-3:2009. *Aluminum and aluminum alloys. Chemical composition and types of plastically processed products. Part 3: Chemical composition and types of products.*

9. PN-EN ISO 6947:1999. *Welding and related processes - Welding positions.*
10. Banasik, M. & Stano, S. Lasery dyskowe – źródło ciepła dla procesów spawalniczych. [In Polish: Disc lasers - a source of heat for welding processes]. *Przegląd Spawalnictwa.* 2011. Vol. 1. P. 17-21.
11. Karcz, K. & Konieczny, J. & Labisz, K. & Gołombek, K. & Janicki, D. Dissimilar steel-to-aluminum joint structure made in laser welding technology. *Acta Physica Polonica A.* 2019. Vol. 135(2). P. 187-192.
12. Silva, M.S. & Barbosa, C. & Acselrad, O. & Pereira, L.C. Effect of chemical composition variation on microstructure and mechanical properties of a 6060 aluminum alloy. *Journal of Materials Engineering and Performance.* 2004. Vol. 13(2). P. 129-134.
13. Liu, B. & Yang, Q. & Wang, Y. Interaction and intermetallic phase formation between aluminum and stainless steel. *Results in Physics.* 2019. Vol. 12. P. 514-524.
14. Yang, J. & Li, Yu-L. & Zhang, H. Microstructure and mechanical properties of pulsed laser welded Al/steel dissimilar joint. *Trans. Nonferrous Met. Soc. China* 2016. Vol. 26. P. 994-1002.
15. Mathieu, A. & Pontevicci S. Laser brazing of a steel/ aluminium assembly with hot filler wire (88% Al, 12% Si). *Materials Science and Engineering A.* 2006. Vol. 435-436. P. 19-28.
16. Yin, F-Ch. & Zhao, M-X. & Liu, Y-X. & Han, W. & Li, Z. Effect of Si on growth kinetics of intermetallic compounds during reaction between solid iron and molten aluminum. *Trans. Nonferrous Met. Soc. China* 2013. Vol. 23. P. 556-561.
17. Mecoa, S. & Pardala, G. & Gangulya, S. & Williamsa, S. & McPherson, N. Application of laser in seam welding of dissimilar steel to aluminium joints for thick structural components. *Optics and Lasers in Engineering* 2015. Vol. 67. P. 22-30.
18. Bruckner, J. Der Cold Metal Transfer (CMT) - Prozess von Stahl/Alu Verbindungen und seine Moglichkeiten. [In German: The Cold Metal Transfer (CMT) process of steel/aluminium connections and its possibilities]. *Schweiss und Pruftechnik*. 2005. No. 10. P. 147-149.
19. Wang, D. & Wang, H. & Cui, H. & He, G. Enhancement of the laser welded AA6061-carbon steel joints by usingAl5Si intermediate layer. *Journal of Materials Processing Technology*. 2016. Vol. 237. P. 277-285.
20. Atabaki, M.M. & Nikodinovski, M. & Chenier, P. & Ma, J. & Harooni, M. & Kovacevic, R. Welding of Aluminum Alloys to Steels: An Overview. *J. Manuf. Sci. Prod.* 2014. Vol. 14(2). P. 59-78.
21. Yeremenko, V.N. & Natanzon, Y.V. & Dybkov, V.I. The effect of dissolution on the growth of the Fe_2Al_5 interlayer in the solid iron-liquid aluminium system. *Journal of Mater Sci*. 1981. Vol. 16(7). P. 1748-1756.
22. Wagner, C. The evaluation of data obtained with diffusion couples of binary single phase and multiphase systems. *Acta Metall.* 1969. Vol. 17(2). P. 99-107.
23. Meco, S. & Cozzolino, L. & Ganguly, S. & Williams, S. & McPherson, N. Laser welding of steel to aluminium: Thermal modelling and joint strength analysis. *Journal of Materials Processing Tech.* 2017. Vol. 247. P. 121-133.

Received 27.10.2020; accepted in revised form 10.03.2022